Supporting Information: Giant anisotropic piezoresponse of layered $ZrSe_3$

Borna Radatović [1,2‡], Hao Li[3*‡], Roberto D'Agosta[4,5], Andres Castellanos-Gomez [1*]*

[1] 2D Foundry research group, Instituto de Ciencia de Materiales de Madrid (ICMM-CSIC), 28049 Madrid, Spain

[2] Department of Inorganic Chemistry, University of Chemistry and Technology Prague, 166 28 Prague 6, Czech Republic

[3] Nanoscale Physics and Devices Laboratory, The Institute of Physics, Chinese Academy of Sciences. P.O.Box 603, 100190 Beijing, China

[4] Nano-Bio Spectroscopy Group and European Theoretical Spectroscopy Facility (ETSF), Departamento de Polimeros y Materiales Avanzados: Fisica, Quimica y Tecnologia, Universidad del Pais Vasco (UPV/EHU), Avenida de Tolosa 72, E-20018 San Sebastian;

[5] Ikerbasque, Basque Foundation for Science, Plaza de Euskadi 5, E-48009 Bilbao, Spain

E-mail: bradatovic@ifs.hr; hao.li@iphy.ac.cn; andres.castellanos@csic.es

‡ Both authors contributed equally to this work

Raman spectroscopy was performed to identify the crystalline orientations of the target flake, as shown in Figure S1. The characteristic peaks A_g^6 (near 230 cm^{-1}) and A_g^8 (near 300 cm^{-1})

reach a maximum when the polarization of the laser is aligned perpendicular to the long-cleaved edge of the flake, corresponding to the b-axis crystalline orientation.

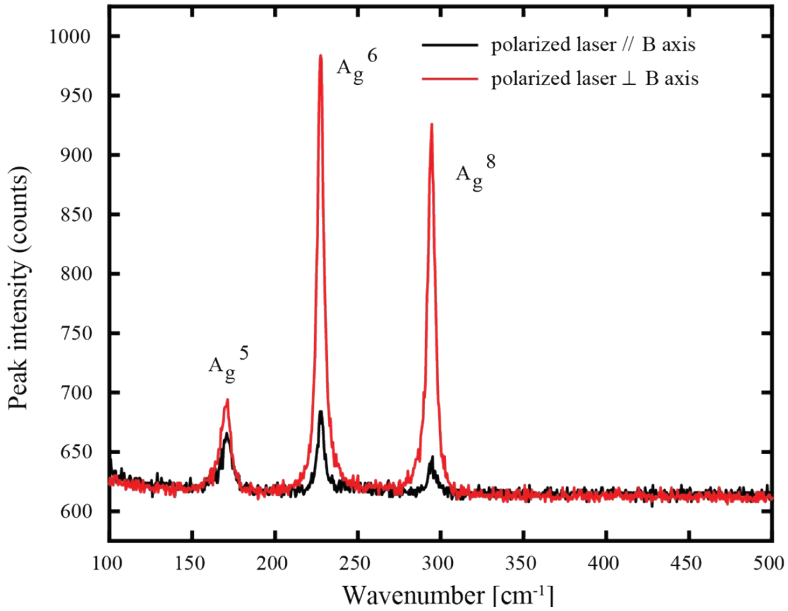

Figure S1. Raman spectrum with polarized laser parallel and perpendicular to B axis.

Following the tensile strain tests of the sample with the b-axis across the channel, shown in Figure 1 (c), we measured electrical transport between electrodes with applied compressive strain along different crystal directions. In contrast to tensile strain, compressive strain results in increased current as the resistance reduces on higher amounts of strain, as shown in Figure S2 (a). Figure S2 (b) summarizes the strain dependent change in resistance under uniaxial compression along different directions. Again, like with the tensile strain, the most significant change in the resistance is observed with the strain applied along the b-axis and minimal when applied in the perpendicular direction. However, compression results in a smaller anisotropy ratio of AR_C = 64% compared to tension. We derived maximum piezoresponse gauge factor $GF_{C\ b\text{-}axis}$ = -44.1 with the strain along the b-axis and minimum $GF_{C\ a\text{-}axis}$ = -9.8 with the strain along the a-axis, as depicted in Figure S2 (c) that shows the dependence of the piezoresponse gauge factor on the direction along which uniaxial compression is applied.

Subsequently, we inspected the device with the configuration in which the a-axis spans across the channel, as shown in Figure 1 (d). Once more, we performed tensile and compressive strain tests while measuring the electrical transport, and again, we observed the same piezoresponse trends. Under tension, resistance increases, while under compression decreases, as shown in Figures S3 (a) and S4 (a). As previously, the highest change in the resistance is caused when the strain is applied along the b-axis and gradually lowers when the strain is applied towards the a-axis, as depicted in Figures S3 (b) and S4 (b). Although we observed the same trends as with the b-axis bridging the channel, both tensile and compressive strain results in lower anisotropy ratios of AR=50% when the a-axis spans across the electrodes. For tensile strain, we derived the maximum piezoresponse gauge factor of $GF_{T\ b\text{-}axis} = 45$ and a minimum of $GF_{T\ a\text{-}axis} = 15$, as depicted in Figure S3 (c). While for compressive strain, we obtained a maximum of $GF_{C\ b\text{-}axis} = -24$ and a minimum of $GF_{C\ a\text{-}axis} = -8$, as depicted in Figure S4 (c).

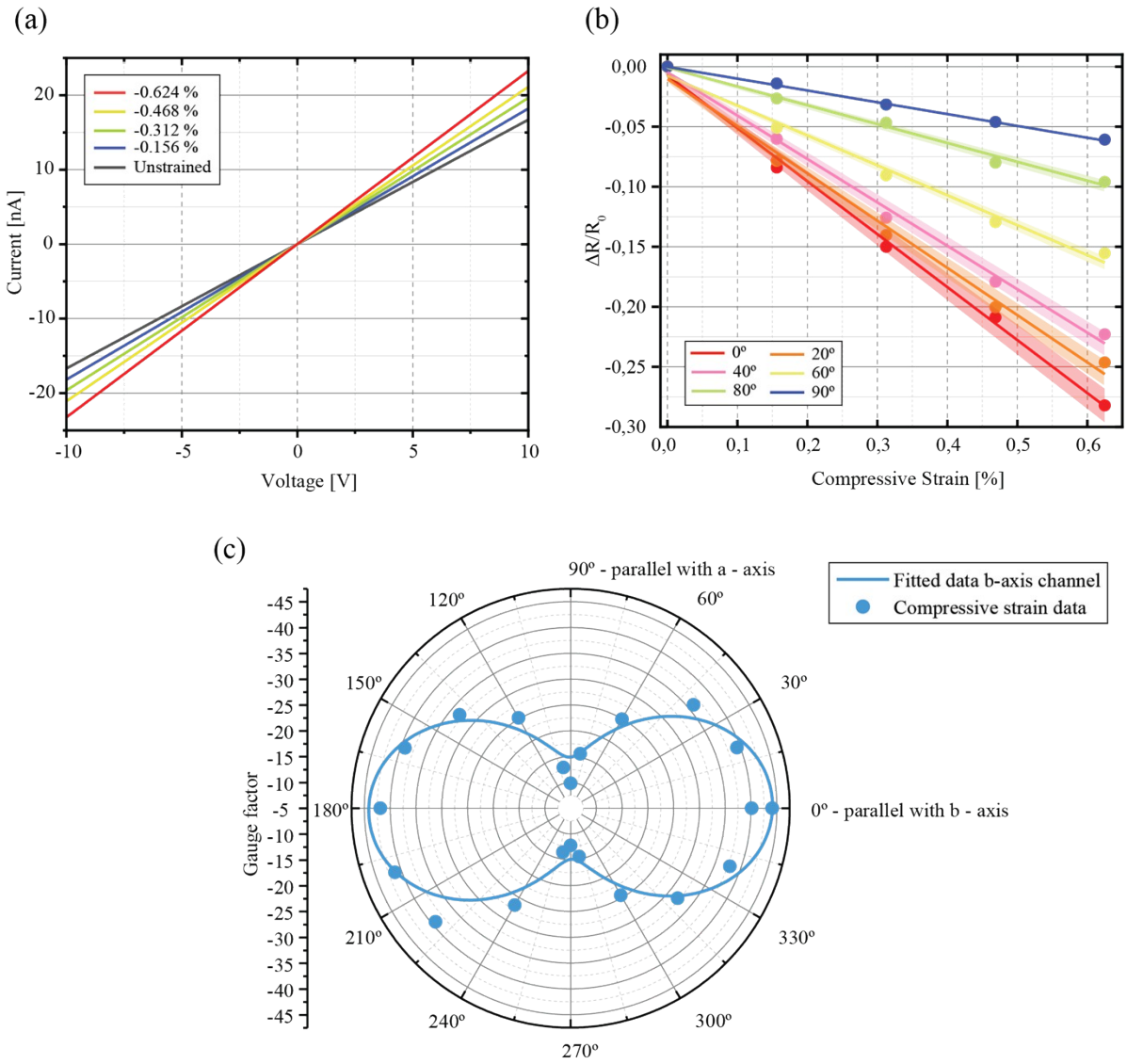

Figure S2. Anisotropic piezoresponse under compressive strain for b-axis over electrodes configuration. (a) IV curves of the $ZrSe_3$ device under different compressive strain, applied along 0°, i.e. b-axis. The current increases as the resistance decreases on the higher amount of the uniaxial compressive strain. (b) The ratio of the relative change of the resistance vs applied compressive strain along different directions. The change of the electrical resistance is most significant when the strain is applied along the 0°, i.e. b-axis and decreases gradually on minimum value when the strain is applied along the 90° – i.e. a-axis. The gauge factor is represented as the slope of the linear fitted lines. (c) Polar plot of the gauge factor changes as a

function of rotating angle from 0° to 360°. 0° means strain parallel to the b-axis, and 90° means strain perpendicular to the b-axis.

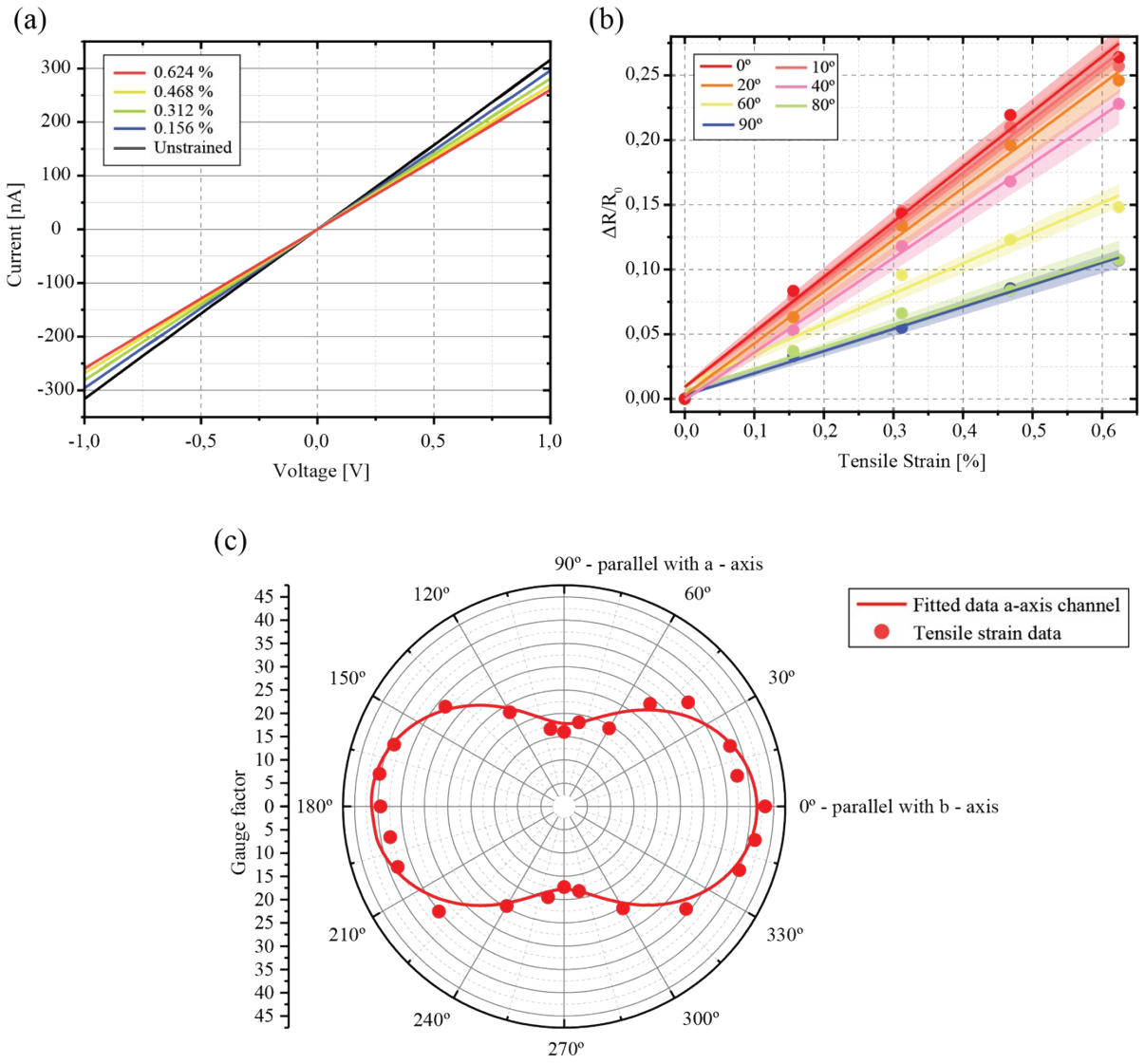

Figure S3. Anisotropic piezoresponse under tensile strain for a-axis over electrodes configuration. (a) IV curves of the $ZrSe_3$ device under different tensile strain, applied along 0°, i.e. b-axis. The current decreases as the resistance increases on the higher amount of the uniaxial tensile strain. (b) The ratio of the relative change of the resistance vs applied tensile strain along different directions. The change of the electrical resistance is most significant when the strain is applied along the 0°, i.e. b-axis and decreases gradually on minimum value when the strain

is applied along the 90° – i.e. a-axis. The gauge factor is represented as the slope of the linear fitted lines. (c) Polar plot of the gauge factor changes as a function of rotating angle from 0° to 360°. 0° means strain parallel to the b-axis, and 90° means strain perpendicular to the b-axis.

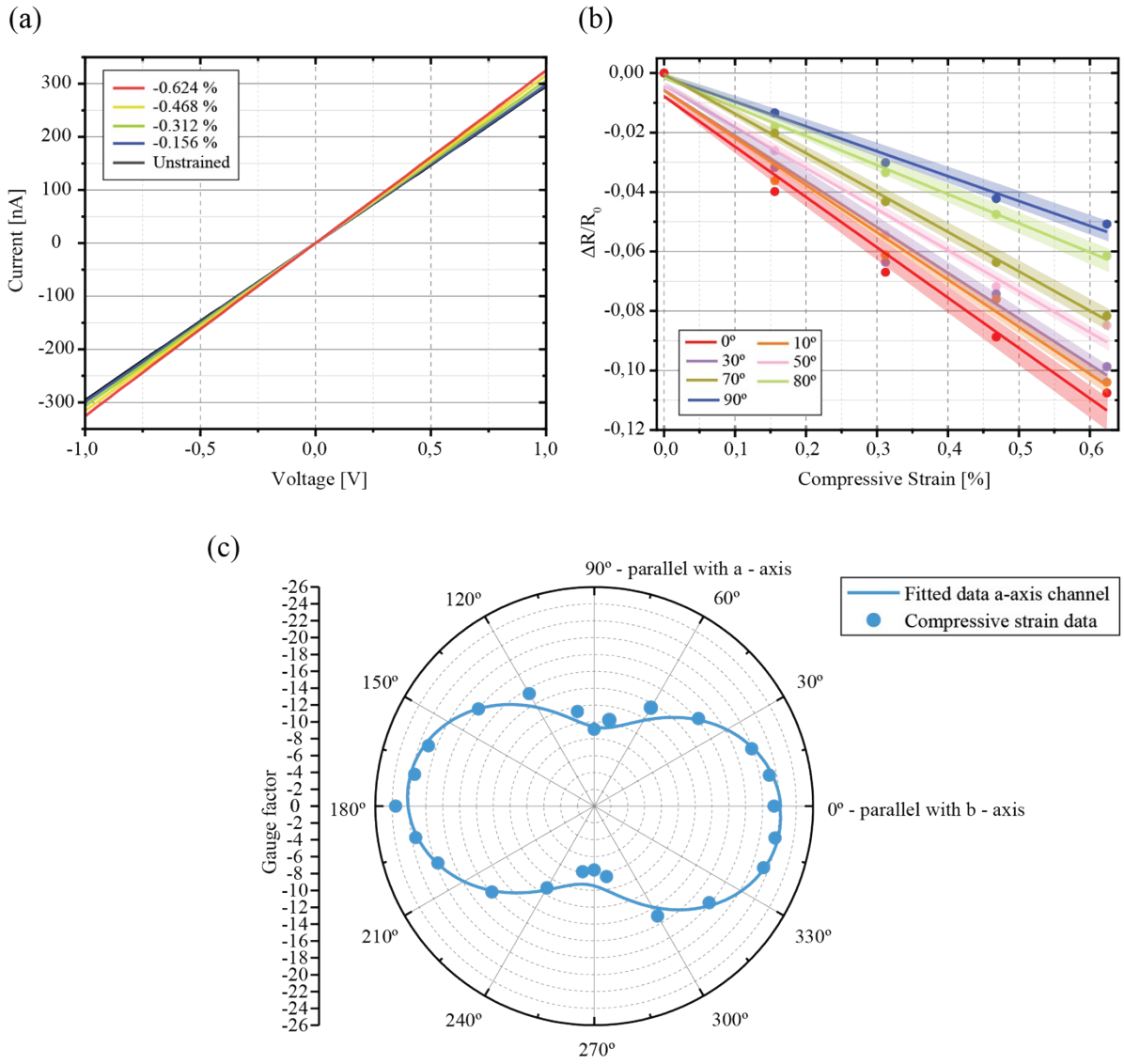

Figure S4. Anisotropic piezoresponse under compressive strain for a-axis over electrodes configuration. (a) IV curves of the $ZrSe_3$ device under different compressive strain, applied along 0°, i.e. b-axis. The current increases as the resistance decreases on the higher amount of the uniaxial compressive strain. (b) The ratio of the relative change of the resistance vs applied compressive strain along different directions. The change of the electrical resistance is most significant when the strain is applied along the 0°, i.e. b-axis and decreases gradually on

minimum value when the strain is applied along the 90° – i.e. a-axis. The gauge factor is represented as the slope of the linear fitted lines. (c) Polar plot of the gauge factor changes as a function of rotating angle from 0° to 360°. 0° means strain parallel to the b-axis, and 90° means strain perpendicular to the b-axis.

Raman spectroscopy was performed with applied tensile strain, parallel and perpendicular to the b-axis, as shown in Figure S5 (a) and (b), respectively. We have used a laser with a wavelength of 532 nm with a power of 0.129 mW and spot size of 2 μm, acquisition time of 20 s and 50× objective. The tensile strain was applied via three point bending setup up to 0,65% with a 0.13% step. We notice that the peak positions of the Raman modes A_g^5, A_g^6, and A_g^8 undergo clear redshift with applied tensile strain. As shown in Figure S5 (c), applying strain along the b-axis causes a larger redshift for all three modes, while perpendicular application of strain leads to a smaller redshift. We notice laser-induced damage to $ZrSe_3$ after longer exposure of the same spot, so we limit our result interpretation without comparing GFs for each Raman mode, as we cannot assess at which moment and the amount that this damage influences acquired Raman spectra.

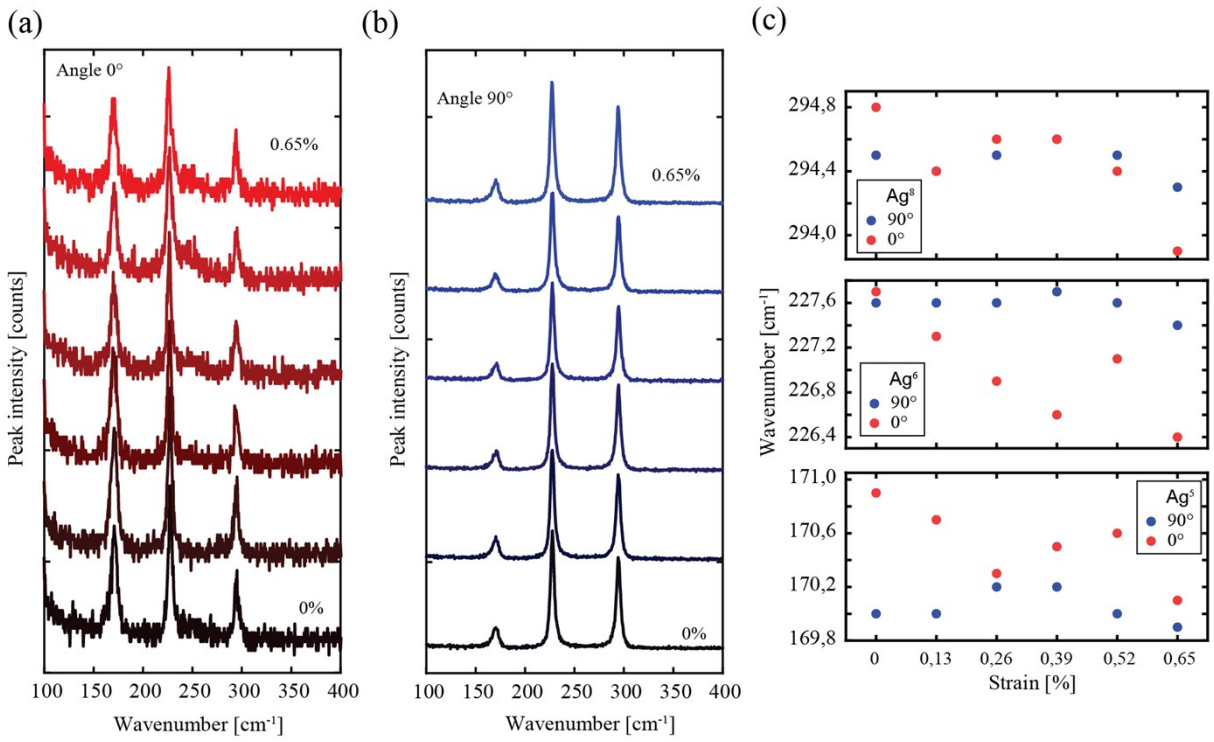

Figure S5. Raman spectroscopy of $ZrSe_3$ under tensile strain applied via three-point bending setup. (a) Raman spectra of $ZrSe_3$ with increasing tensile strain applied along the b-axis of the flake. (b) Raman spectra of $ZrSe_3$ with increasing tensile strain applied perpendicular to b-axis of the flake. (c) Raman shifts of modes A_g^5, A_g^6, and A_g^8 as a function of the applied uniaxial tensile strain parallel and perpendicular to b axis respectively. Note that, angle 0º represents strain applied along b axis (red dots) while angle 90º represents that strain is applied perpendicular to b axis (blue dots).